THEORETICAL STUDY OF GROUND STATE PROPERTIES OF Na^+, Cs^+, Mg^{2+} AND Ba^{2+} DOPED MAYENITE AND ITS ELECTRIDE FORMS UNDER EXTREME CONDITIONS

Milan Pejić[1,2,3*], Dejan Zagorac[1,2], Jelena Zagorac[1,2], Tamara Škundrić[1,2,4], Branko Matović[1,2]

[1] Institute of Nuclear Sciences "Vinča", University of Belgrade, Belgrade, Serbia
[2] Centre of Excellence "CextremeLab", Centre for synthesis, processing and characterization of materials for application in the extreme conditions, Belgrade, Serbia
[3] Department of Physics, Faculty of Physics, University of Belgrade, Belgrade, Serbia
[4] Department of Chemistry, Faculty of Science and Mathematics, University of Niš, Niš, Serbia
Corresponding author: milan.pejic@vinca.rs*

Abstract: *Calculations of band structure and electronic density distribution near Fermi energy have been performed for complex nanoporous oxide mayenite $12CaO{\cdot}7Al_2O_3$ (C12A7) on the ab initio level. The electronic structure of mayenite doped with selected cations from the 1st and 2nd group of the periodic table of elements (Na^+, Cs^+, Mg^{2+}, and Ba^{2+}) have also been calculated in order to estimate the effect of cationic doping on structural, electronic, and optical properties of mayenite. Partial and complete substitution of the interstitial oxygen anions (there are two O^{2-} anions per unit cell) with electrons (e^- "doping") is also considered in ab initio calculations to observe differences in electronic structure (such as band gap and Fermi level) during the transition from insulator (regular mayenite crystal with O^{2-} anions in interstitial places) to electride.*

Keywords: mayenite, DFT, ab-initio, electronic band structure, cation doping, electride, transparent conductors.

1. Introduction

Mayenite ($12CaO{\cdot}7Al_2O_3$, $Ca_{12}Al_{14}O_{33}$, C12A7 or C12A7:$(O^{2-})_2$) belongs to a group of calcium aluminates, a range of minerals obtained, by heating calcium oxide and aluminium oxide together at high temperatures, or recently in various ways, from solution-derived precursors to plasma arc melting.[1-8] It crystallizes with a body-centered cubic crystal structure belonging to the space group No. 220, *I43d*, with a unit cell of about 12 Å and with Z=2 (two formula units per unit cell).[9-11] It is comprised of nano-pores and polyhedra that form cages (similar to zeolites) which are approximately 4-5Å in diameter.

The unit cell of C12A7 consists of 12 cages formed by the Ca-Al-O framework, which include 24 Ca, 28 Al and 64 O atoms, while the remaining two oxygen anions are randomly distributed within the cages as extra-framework ions (see Figure 1). Cages with different S4 symmetry axes (S_{4x}, S_{4y}, and S_{4z}), which pass through two Ca (axial) atoms, are connected via large windows formed by a shared Ca-Al-O framework. This means that in the C12A7 unit cell structure, two oxygen ions occupy two of the twelve cages, which are also responsible for the high oxygen ion conductivity found in mayenite.[12] The structure is known as a host material to a variety of anionic species such as O^-, O^{2-}, e^-, OH^-, H^-, F^-, and

Cl^-. [12-16] On the other hand, there has been a plethora of studies on the cationic doping of C12A7 $(Ca_{24}Al_{28}O_{64})^{4+}$, where substitutional cation is located on the Ca^{2+} or Al^{3+} site.[12, 17-19] Doping affects emissive, optical, and chemical properties of mayenite where an important role is played by the structure-property relationships while cationic dopants have strong impacts on the electronic properties and structural distortions.[12, 20]

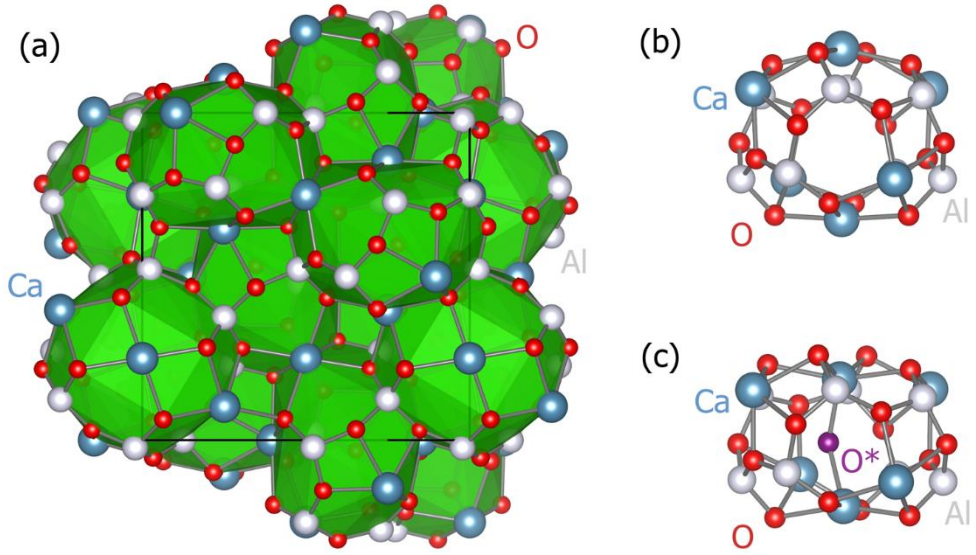

Figure 1. Mayenite structure: (a) C12A7 unit cell, consisting of 12 cages formed by Ca-Al-O framework, (b) Mayenite cage without extra-framework species, (c) Cage containing extra-framework O^{2-} ion (O*).

Many of mayenite's properties that are uncharacteristic to $CaO\text{-}Al_2O_3$ systems are the result of its unusual structure.[21] It has a melting point of 1415°C, and its "electride"[22] (mayenite with all interstitial O^{2-} ions substituted with electrons, which then serve as anions) state can be also regarded as a chemically and thermally stable structure.[15] Varying the electron concentration in the electride form of mayenite can be used to make it optically transparent and electrically conductive material.[23] Conductivity and thermodynamic stability of anion-substituted[20, 24] and cation-substituted[12, 25] mayenite are also being studied recently. There are many other applications of mayenite ranging from catalysts, batteries, hydrogen storage, and transportation to environmental applications, cement, ceramic, and bio-materials.[12, 20, 26-30]

Theoretical modeling of C12A7 and its modifications represents a formidable challenge in the search for novel transparent conducting oxides, catalysts, anion conductors, etc. because of the size of the unit cell and random arrangement of extra-framework species. The purpose of this work is to generate structural models of chosen cation-doped bulk C12A7 structures and analyze their electronic properties using quantum-mechanical simulations based on density-functional theory (DFT). Moreover, this study investigates the behavior of mayenite structure at extreme conditions as a function of the size, charge, and position of the doped cation.

2. Details of the Calculations

Our general approach to the investigation of advanced materials as the effect of anion/cation substitution is given elsewhere [31-36]. Similarly, the effect of extreme conditions on structural and electronic properties, as well as the structure-property relationship has been studied previously[37-44] and is of great importance. In this study, structural and electronic properties of mayenite (C12A7 or C12A7:$(O^{2-})_2$), Na-doped Mayenite (C12A7+Na or C12A7:$(O^{2-})_2$(Na)), Mg-doped (C12A7+Mg or C12A7:$(O^{2-})_2$(Mg)), Cs-doped (C12A7+Cs or C12A7:$(O^{2-})_2$(Cs)) and Ba-doped (C12A7+Ba or C12A7:$(O^{2-})_2$(Ba)) structures (C12A7+X represents two mayenite formula units doped with one X cation), as well as partial (C12A7:$(O^{2-})(e^-)_2$) and complete mayenite electride (C12A7:$(e^-)_4$), are analyzed using quantum-mechanical simulations based on density-functional theory (DFT).

Generalized Gradient Approximation (GGA) with the PBE (Perdew, Burke, and Ernzerhof) functional,[45] as implemented in VASP[46, 47] and Quantum Espresso (QE)[48, 49] simulation package were used in the calculations. Plane-wave basis set with 50 Ry (550 eV) kinetic energy cut-off for wavefunctions, 500 Ry cut-off for charge density and potential, and 4 x 4 x 4 Monkhorst-Pack grids for k-point sampling were used. The structures were fully optimized using both VASP and QE software packages, while the electronic properties were calculated using the QE code. Visualization of the structures and cages was done by VESTA software.[50]

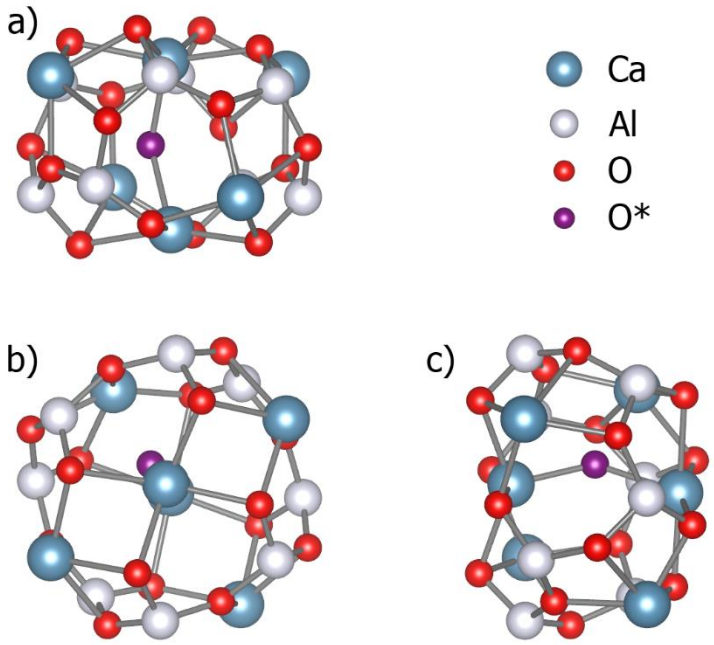

Figure 2. Mayenite C12A7:$(O^{2-})_2$ cage with extra-framework O^{2-} anion structure: (a) front, (b) top, and (c) side view. Calculations performed using GGA-PBE functional.

3. Results and Discussion

3a. Structure properties

The ground state of mayenite C12A7 cages with extra-framework O^{2-} anion structure obtained by DFT calculations is shown in Figure 2. Structural relaxation of the structure using GGA-PBE functional resulted in the unit cell of a=12.065 Å (Table 1). Present

calculations with O^{2-} anion placed in an empty cage is in good agreement with already existing experimental and theoretical results.[9, 21, 22, 51-57] In the following, we investigate the influence of cation doping on the mayenite C12A7 structure. In particular, this was performed by doping C12A7+X (X = Mg, Na, Ba, Cs), where dopant cations are initially incorporated inside the various position of the empty cage or in the framework as an extra-framework species (Figure 1b), pushing the mayenite cage to the extreme boundaries. Thus, each C12A7+X (X = Mg, Na, Ba, Cs) cation doped calculation consists of nine empty mayenite cages (cage without extra-framework species, Figure 1b), one previously "empty" cage that is filled with doped X atom (X = Mg, Na, Ba, Cs), and two already existing interstitial oxygen anions inside two other cages (Figure 1c), making in total twelve mayenite C12A7 cages.

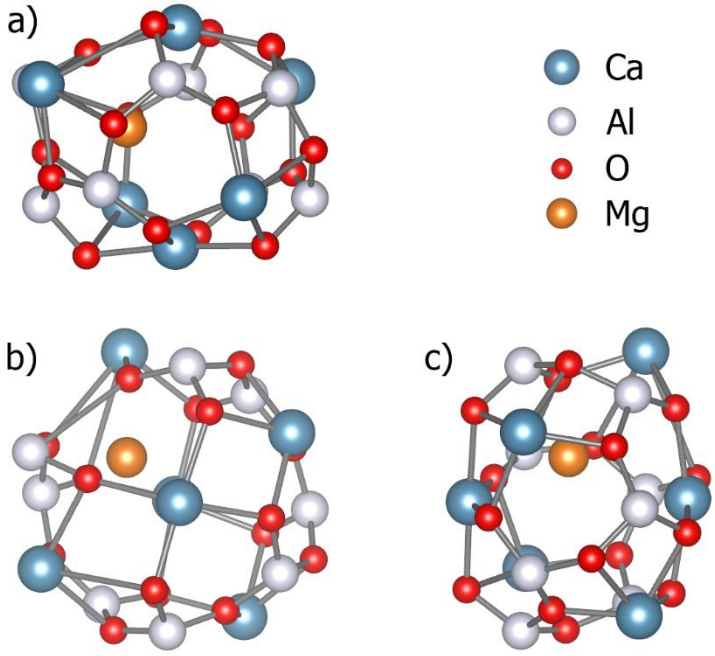

Figure 3. Mg-doped mayenite C12A7:$(O^{2-})_2$(Mg) cage with extra-framework Mg cation structure: (a) front, (b) top, and (c) side view. Calculations performed using GGA-PBE functional.

Firstly, we have investigated an Mg^{2+} cation doping on C12A7:$(O^{2-})_2$ mayenite structure. The resulting Mg-doped mayenite C12A7:$(O^{2-})_2$(Mg) cage with extra-framework Mg cation structure calculated using GGA-PBE is shown in Figure 3. The Mg atom has the same oxidation number as Ca^{2+} and it is its closely related element from the Group 2A (or IIA) of the periodic table (the alkaline earth metals), but the ionic radius is much smaller than calcium (Ca).[58] Interestingly, the ground state structure is achieved with dopant Mg cations incorporated inside the cages, even when Mg atoms were placed at Ca cation sites in the C12A7 framework (Figure 3). The calculated unit cell of a = 12.088 Å and volume V = 1766.14 $Å^3$ are larger than the undoped C12A7:$(O^{2-})_2$ mayenite structure (Table 1).

The influence of the Na cation doping on the C12A7:$(O^{2-})_2$ mayenite structure has been investigated in the next phase of the study. Figure 4 shows the Na-doped mayenite C12A7:$(O^{2-})_2$(Na) cage with extra-framework Na cation structure calculated using GGA-PBE functional. The sodium (Na) atom has an oxidation number of +1 and comes from Group 1 elements (alkali metals) of the periodic table, differently from calcium atoms. On the other hand, the ionic radius of the Na cation is very close to calcium,[58] while sodium and

magnesium are members of the s-block of the third period of the periodic table. The computed unit cell of a = 12.090 Å and volume V = 1767.08 $Å^3$ is just a bit larger than the Mg-doped mayenite C12A7:$(O^{2-})_2$(Mg) cage structure (Table 1). As previously observed, the ground state is achieved with dopant Na cations incorporated inside the cages as extra-framework species (Figure 4).

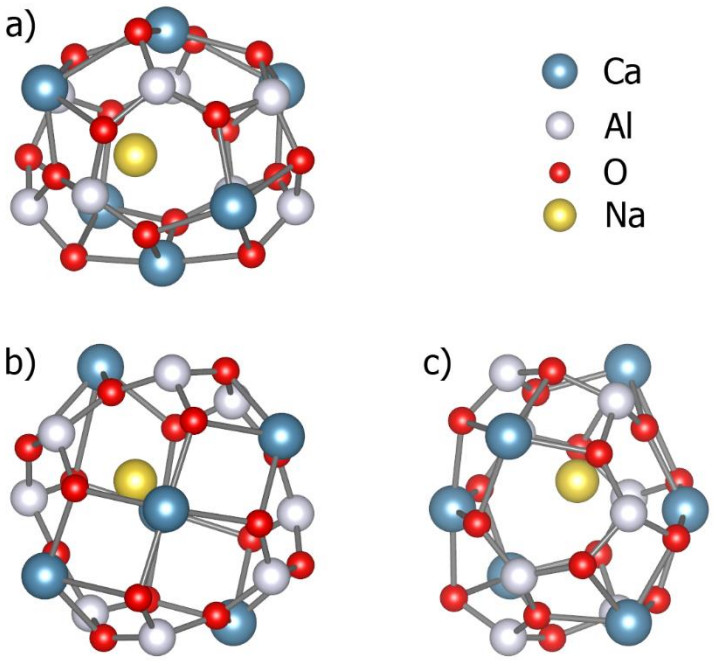

Figure 4. Na-doped mayenite C12A7:$(O^{2-})_2$(Na) cage with extra-framework Na cation structure: (a) front, (b) top, and (c) side view. Calculations performed using GGA-PBE functional.

In the case of the barium (Ba) cation doping on C12A7:$(O^{2-})_2$ mayenite structure, Figure 5 shows the resulting Ba-doped mayenite C12A7:$(O^{2-})_2$(Na) cage with extra-framework Ba cation structure calculated using GGA-PBE functional. The Ba atom has the same oxidation number as Ca^{2+} and it is also a closely related element from the Group 2A (or IIA) of the periodic table (as is the magnesium atom). However, the ionic radius of the Ba cation is much larger compared to calcium (Ca) and especially the Mg cation.[58] The calculated cell parameter of a = 12.116 Å and volume of V = 1778.74 $Å^3$ is larger than undoped and Mg-doped mayenite C12A7:$(O^{2-})_2$(Mg) cage structure (Table 1), as expected. Still, even with incorporating a much larger Ba atom, the ground state is achieved with dopant Ba cations inside the cages as extra-framework species as previously observed (Figure 5).

Finally, the influence of the cesium cation doping on C12A7:$(O^{2-})_2$ mayenite structure has been investigated in great detail. Figure 6 shows the cesium (Cs) cation doping on C12A7:$(O^{2-})_2$ mayenite structure, resulting in C12A7:$(O^{2-})_2$(Cs) cage with extra-framework Cs cation structure calculated using GGA-PBE functional. The cesium cation has an oxidation number +1 and comes from Group 1 elements of the periodic table (same as Na), different than that of the calcium atoms. Moreover, Cs atoms are the largest with the highest ionic radii, compared to Ca or any of the other dopant atoms.[58] Still, DFT calculations show that the calculated cell parameter of a = 12.111 Å and volume of V = 1776.24$Å^3$ are a bit smaller than Ba-doped mayenite C12A7:$(O^{2-})_2$(Ba) cage structure (Table 1). By

incorporating even larger Cs atoms with a different charge, the ground state is achieved with dopant Cs cations inside the cages as extra-framework species as in all previous cases (Figure 6).

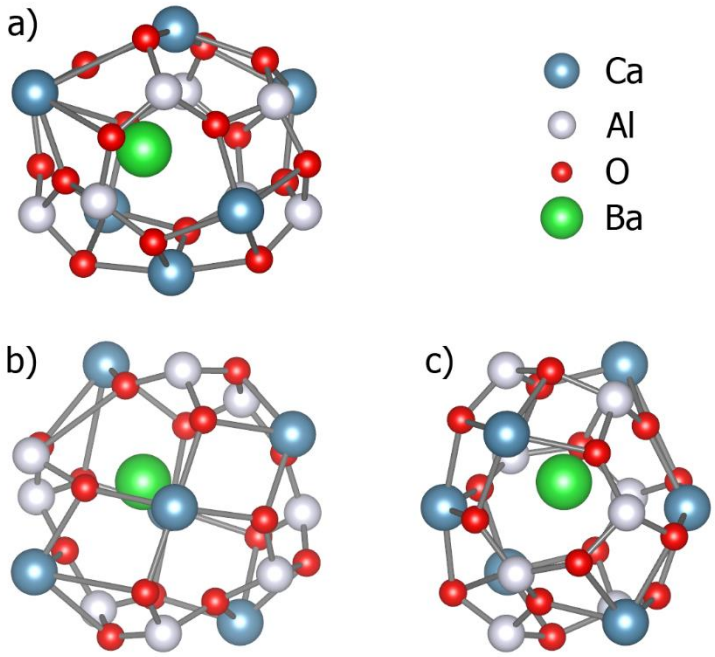

Figure 5. Ba-doped mayenite C12A7:$(O^{2-})_2$(Ba) cage with extra-framework Ba cation structure: (a) front, (b) top, and (c) side view. Calculations performed using GGA-PBE functional.

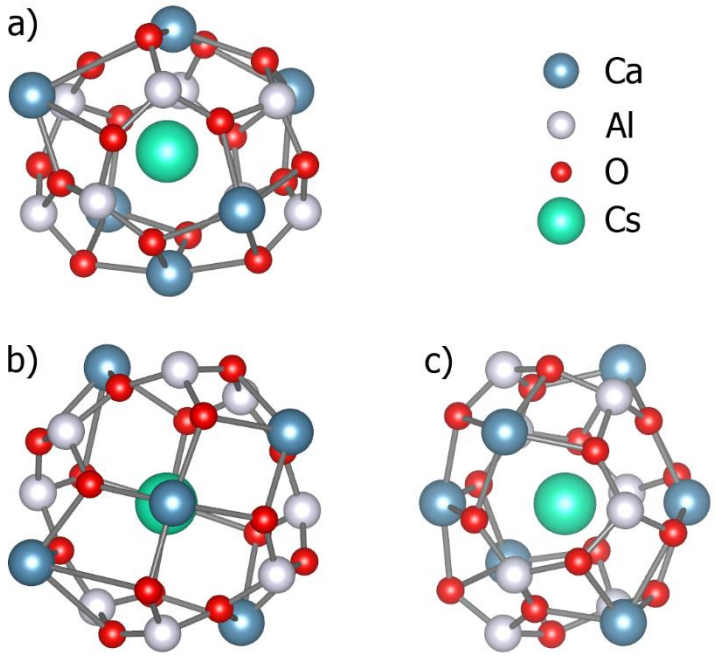

Figure 6. Cs-doped mayenite C12A7:$(O^{2-})_2$(Cs) cage with extra-framework Cs cation structure: (a) front, (b) top, and (c) side view. Calculations performed using GGA-PBE functional.

In summary, for all cation-doped configurations, C12A7+X, the ground state is achieved with dopant cations incorporated inside the cages as extra-framework species, along with two already existing interstitial oxygen anions inside two other cages (Figures 3-6). Having a cation at the interstitial ion place, as expected, deforms the cage in the opposite way the anion does. All cation-doped cages are elongated in the axial Ca-Ca direction, with the Mg-containing cage exhibiting the smallest change compared to the oxygen-containing cage, as well as compared to the cage without extra-framework species. Cages that have Ba and Cs as extra-framework species exhibit the largest elongation along the axial Ca-Ca direction. Theoretical models of all doped mayenite structures show that the basic structure of the lattice framework remains unchanged.

Table 1. Mayenite and Na-, Mg-, Cs-, and Ba-doped mayenite structure parameters calculated using GGA-PBE functional.

Structure	a [Å]	V [Å^3]	Density [g/cm^3]	Ca-Ca distance* [Å]	Ca-X-Ca angle [°]
C12A7:$(O^{2-})_2$	12.065	1756.15	2.62	4.26	141.3
C12A7:$(O^{2-})_2$(Mg)	12.088	1766.14	2.63	5.54	116.7
C12A7:$(O^{2-})_2$(Na)	12.090	1767.08	2.63	5.92	141.8
C12A7:$(O^{2-})_2$(Ba)	12.116	1778.74	2.72	6.20	144.4
C12A7:$(O^{2-})_2$(Cs)	12.111	1776.24	2.72	6.22	175.8

* Axial Ca-Ca distance in the cages containing interstitial atoms (O, Na, Mg, Cs or Ba). Ca-Ca distance in cages without interstitial atoms (empty cages) ranges from ~5.6Å to ~5.9Å.

3b. Electronic properties

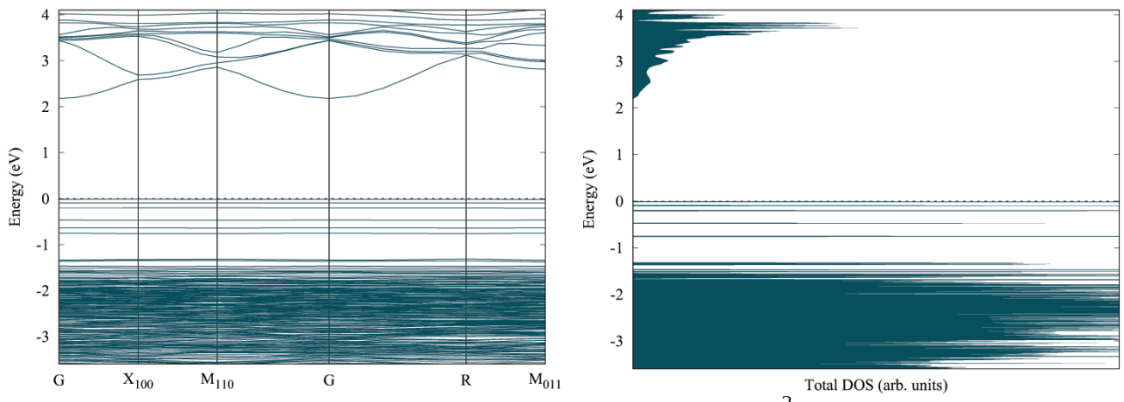

Figure 7. Electronic band structure and DOS for C12A7:$(O^{2-})_2$ mayenite calculated using GGA-PBE functional.

In order to investigate the electronic properties of doped mayenite structures, we have performed electronic band structure and Density of States (DOS) calculations. Figure 7 shows the electronic band structure and DOS for undoped C12A7:$(O^{2-})_2$ mayenite calculated

using GGA-PBE functional. Our results show the existence of the direct band gap for insulator-type mayenite structure ($C12A7:(O^{2-})_2$) of the order of 2 eV in agreement with previous experimental and theoretical studies. [9, 21, 22, 51-57] In addition, we have computed the total DOS for $C12A7:(O^{2-})(e^-)_2$ partial electride and $C12A7:(e^-)_4$ electride shown in Figure 8. The DOS calculations show that both electride mayenite structures appear to have a metallic character.

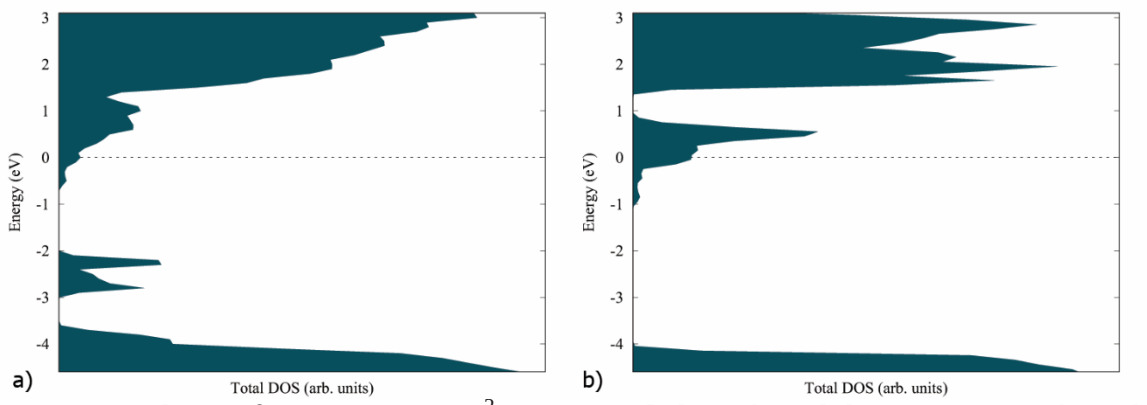

Figure 8. Total DOS for: (a) $C12A7:(O^{2-})(e^-)_2$ partial electride and (b) $C12A7:(e^-)_4$ electride.

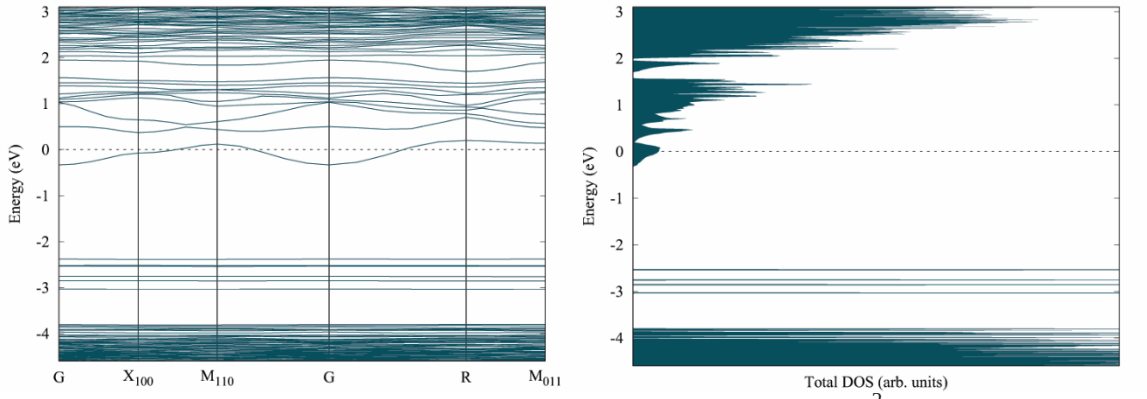

Figure 9. Electronic band structure and DOS for Na doped $C12A7:(O^{2-})_2(Na)$ mayenite.

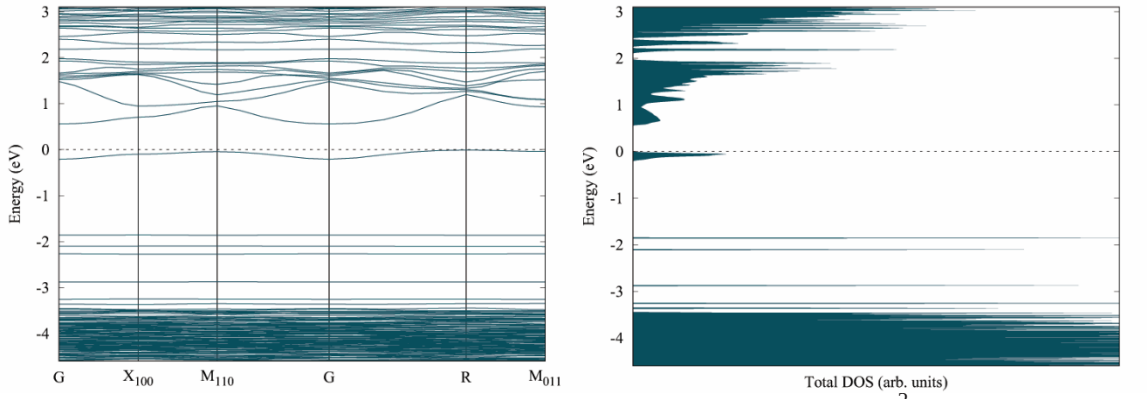

Figure 10. Electronic band structure and DOS for Mg-doped $C12A7:(O^{2-})_2(Mg)$ mayenite.

To investigate the potassium cation-doped mayenite structure, we have computed the electronic band structure and DOS for Na-doped $C12A7:(O^{2-})_2(Na)$ mayenite. It shows that

when the C12A7:$(O^{2-})_2$ mayenite structure is doped with potassium cation within the cage, it appears to be semi-metallic, resembling the electride in Figure 8. On the other hand, when the C12A7:$(O^{2-})_2$ mayenite structure is doped with Mg cation inside the cage (Figure 10), it appears to be semiconducting (similar to the undoped mayenite in Figure 7). Still, the electronic band structure and DOS for Mg-doped C12A7:$(O^{2-})_2$(Mg) mayenite (Figure 10) are showing a much smaller band gap compared to the undoped mayenite (of the order of 0.6 eV).

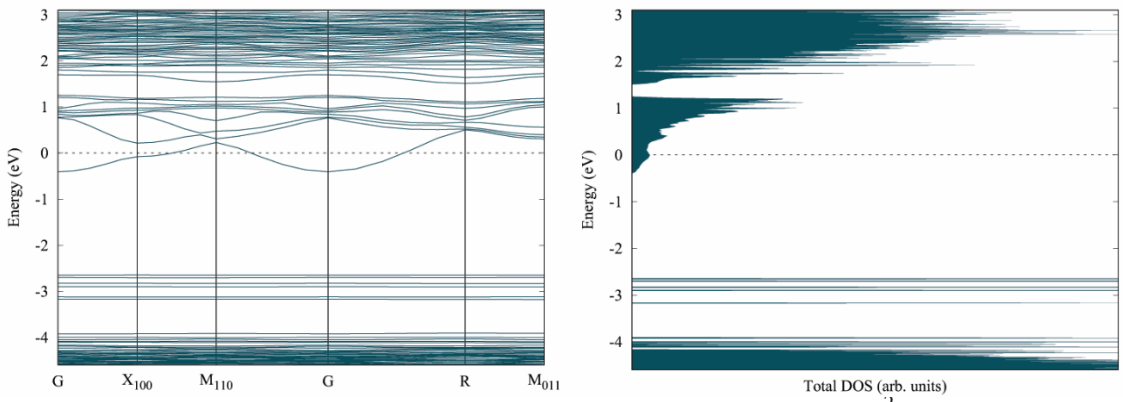

Figure 11. Electronic band structure and DOS for Cs doped C12A7:$(O^{2-})_2$(Cs) mayenite.

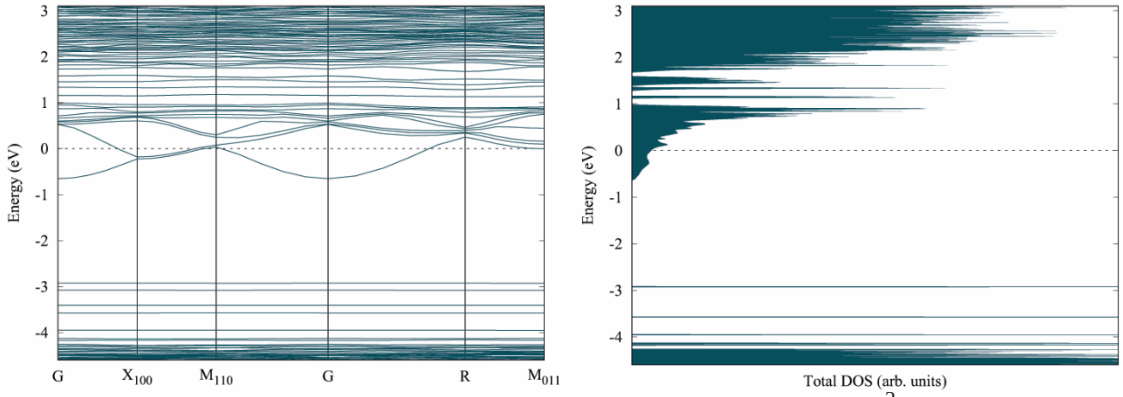

Figure 12. Electronic band structure and DOS for Ba doped C12A7:$(O^{2-})_2$(Ba) mayenite.

Figure 11 shows the electronic band structure and DOS for Cs-doped C12A7:$(O^{2-})_2$(Cs) mayenite computed using GGA-PBE functional. It shows that Cs-doped mayenite appears to be semi-metallic, similar to Na-doped C12A7:$(O^{2-})_2$(Na) mayenite (Figure 9). The electronic band structure and DOS for Ba-doped C12A7:$(O^{2-})_2$(Ba) mayenite is shown in Figure 12. It appears that Ba-doped mayenite exhibits metallic behavior, different from all other dopant cations. The density of states shows a moderately dispersed band at the bottom of the conduction band (similar to the electride DOS). A moderately dispersed band at the bottom of the conduction band which is also separated from the valence band by a large fundamental band gap should favor transparent conducting behavior. To summarize, there is a great diversity of electronic properties of C12A7:$(O^{2-})_2$ mayenite structures, depending on the selection of doping cations.

4. Conclusion

Cationic dopants have strong impacts on electronic properties, and structural distortions. This study investigates the behavior of mayenite structure under extreme conditions as a function of size, charge, and position of the doping cations (Na^{+}, Cs^{+}, Mg^{2+}, and Ba^{2+}). The electron doping increases mayenite electrical conductivity compared to the base mayenite (C12A7:$(O^{2-})_2$). A similar effect is obtained by cationic doping with all chosen cations. While doping (both electronic and cationic) increases conductivity, it also increases the concentration of electrons at the bottom of the conduction band, which leads to stronger optical absorption due to interband transition. There is a trade-off between higher conductivity and transparency in mayenite. Calculations show that C12A7+X (possibly with different cation concentrations) are good candidates for transparent conducting oxides as well as tunable band-gap semiconductors.

Acknowledgments

This research was financially supported by the Ministry of Education, Science, and Technological Development of the Republic of Serbia (Grant No. 1702201).

References

[1] D. Jiang, Z. Zhao, S. Mu, V. Phaneuf, J. Tong, Simple and Efficient Fabrication of Mayenite Electrides from a Solution-Derived Precursor, *Inorganic Chemistry*, 56 (2017) 11702-11709.
[2] K. Berent, S. Komarek, R. Lach, W. Pyda, The Effect of Calcination Temperature on the Structure and Performance of Nanocrystalline Mayenite Powders, *Materials*, 12 (2019) 3476.
[3] F. Li, X. Zhang, H. Liu, Calciothermic synthesis of inorganic [Ca24Al28O64]4+(4e−) electride from solid-derived precursor, *Vacuum*, 169 (2019) 108880.
[4] T. Johnson, E.W. Awin, M.D. Prekajski-Đorđević, B. Matović, R. Kumar, Metal-Like Thermal Conductivity Possessed By Atmosphere Assisted Synthesis, *Journal of Innovative Materials in Extreme Conditions*, 1 (2020) 7-11.
[5] A.V. Kapishnikov, R.M. Kenzhin, A.P. Koskin, A.M. Volodin, P.V. Geydt, Mayenite Synthesis from Hydroxide Precursors: Structure Formation and Active Sites on Its Surface, *Materials*, 15 (2022) 778.
[6] B. Matović, M. Prekajski, J. Pantić, T. Bräuniger, M. Rosić, D. Zagorac, D. Milivojević, Synthesis and densification of single-phase mayenite (C12A7), *Journal of the European Ceramic Society*, 36 (2016) 4237-4241.
[7] S. Weber, S. Schäfer, M. Saccoccio, K. Seidel, H. Kohlmann, R. Gläser, S.A. Schunk, Mayenite-based electride C12A7e−: an innovative synthetic method via plasma arc melting, *Materials Chemistry Frontiers*, 5 (2021) 1301-1314.
[8] E.V. Ilyina, A.F. Bedilo, S.V. Cherepanova, Y.Y. Gerus, E.I. Shuvarakova, A.A. Vedyagin, Aerogel synthesis of calcium aluminates with varied stoichiometry, *Journal of Sol-Gel Science and Technology*, (2022).
[9] L. Palacios, Á.G. De La Torre, S. Bruque, J.L. García-Muñoz, S. García-Granda, D. Sheptyakov, M.A.G. Aranda, Crystal Structures and in-Situ Formation Study of Mayenite Electrides, *Inorganic Chemistry*, 46 (2007) 4167-4176.
[10] T. Sakakura, K. Tanaka, Y. Takenaka, S. Matsuishi, H. Hosono, S. Kishimoto, Determination of the local structure of a cage with an oxygen ion in Ca12Al14O33, *Acta Crystallographica Section B*, 67 (2011) 193-204.

[11] F. Gfeller, 7. Mayenite Ca12Al14O32[X2−]: From minerals to the first stable electride crystals, in: A. Thomas, D. Rosa Micaela (Eds.) *Highlights in Mineralogical Crystallography*, De Gruyter (O), Berlin, München, Boston, 2015, pp. 169-196.
[12] J. R. Salasin, C. Rawn, Structure Property Relationships and Cationic Doping in [Ca24Al28O64]4+ Framework: A Review, *Crystals*, 7 (2017) 143.
[13] J. JEEVARATNAM, F.P. GLASSER, L.S.D. GLASSER, Anion Substitution and Structure of 12CaO·7A122O, *Journal of the American Ceramic Socie*ty, 47 (1964) 105-106.
[14] K. Hayashi, M. Hirano, S. Matsuishi, H. Hosono, Microporous Crystal 12CaO·7Al2O3 Encaging Abundant O- Radicals, *Journal of the American Chemical Society*, 124 (2002) 738-739.
[15] S. Matsuishi, Y. Toda, M. Miyakawa, K. Hayashi, T. Kamiya, M. Hirano, I. Tanaka, H. Hosono, High-Density Electron Anions in a Nanoporous Single Crystal: $[Ca_{24}Al_{28}O_{64}]4^{+}(4e^{-})$, *Science*, 301 (2003) 626-629.
[16] V.I. Zaikovskii, A.M. Volodin, V.O. Stoyanovskii, S.V. Cherepanova, A.A. Vedyagin, Effect of carbon coating on spontaneous C12A7 whisker formation, *Applied Surface Science*, 444 (2018) 336-338.
[17] B. Matović, M.G. Nikolić, M.D. Prekajski-Đorđević, S. Dmitrović, J.M. Luković, J. Maletaškić, B. Jelenković, Luminescence Properties Of Eu3+ Doped Mayenite Under High Pressure, *Journal of Innovative Materials in Extreme Conditions*, 1 (2020) 12-18.
[18] Y. Lv, Y. Sun, J. Xu, X. Xu, A.J. Fernández-Carrión, T. Wei, H. Yi, X. Kuang, Phase Evolution, Electrical Properties, and Conduction Mechanism of Ca12Al14–xGaxO33 ($0 \leq x \leq 14$) Ceramics Synthesized by a Glass Crystallization Method, *Inorganic Chemistry*, 60 (2021) 2446-2456.
[19] K. Hayashi, N. Ueda, S. Matsuishi, M. Hirano, T. Kamiya, H. Hosono, Solid State Syntheses of 12SrO·7Al2O3 and Formation of High Density Oxygen Radical Anions, O^{-} and O^{2-}, *Chemistry of Materials*, 20 (2008) 5987-5996.
[20] H. Visbal, T. Omura, K. Nagashima, T. Itoh, T. Ohwaki, H. Imai, T. Ishigaki, A. Maeno, K. Suzuki, H. Kaji, K. Hirao, Exploring the capability of mayenite (12CaO·7Al2O3) as hydrogen storage material, *Scientific Reports*, 11 (2021) 6278.
[21] P.V. Sushko, A.L. Shluger, M. Hirano, H. Hosono, From Insulator to Electride: A Theoretical Model of Nanoporous Oxide 12CaO·7Al2O3, *Journal of the American Chemical Society*, 129 (2007) 942-951.
[22] Z. Li, J. Yang, J.G. Hou, Q. Zhu, Is Mayenite without Clathrated Oxygen an Inorganic Electride?, *Angewandte Chemie International Edition*, 43 (2004) 6479-6482.
[23] K. Hayashi, S. Matsuishi, T. Kamiya, M. Hirano, H. Hosono, Light-induced conversion of an insulating refractory oxide into a persistent electronic conductor, *Nature*, 419 (2002) 462-465.
[24] J.-P. Eufinger, A. Schmidt, M. Lerch, J. Janek, Novel anion conductors – conductivity, thermodynamic stability and hydration of anion-substituted mayenite-type cage compounds C12A7:X (X = O, OH, Cl, F, CN, S, N), *Physical Chemistry Chemical Physics*, 17 (2015) 6844-6857.
[25] K. Khan, A.k. Tareen, U. Khan, A. Nairan, S. Elshahat, N. Muhammad, M. Saeed, A. Yadav, L. Bibbò, Z. Ouyang, Single step synthesis of highly conductive room-temperature stable cation-substituted mayenite electride target and thin film, *Scientific Reports*, 9 (2019) 4967.
[26] A. Intiso, F. Rossi, A. Proto, R. Cucciniello, The fascinating world of mayenite (Ca12Al14O33) and its derivatives, Rendiconti Lincei. *Scienze Fisiche e Naturali*, 32 (2021) 699-708.
[27] K. Fang, J. Zhao, D. Wang, H. Wang, Z. Dong, Use of ladle furnace slag as supplementary cementitious material before and after modification by rapid air cooling: A comparative study of influence on the properties of blended cement paste, *Construction and Building Materials*, 314 (2022) 125434.
[28] J.G. Miranda-Hernández, C.O. González-Morán, H. Herrera-Hernández, E.H. Sánchez, J.d.J.A. Flores-Cuautle, M. Ortega-Avilés, Sea snail shells for synthesis of ceramic compounds reinforced with metallic oxide: Microstructural, mechanical and electrical behavior, *Materials Today Communications*, 28 (2021) 102656.
[29] E. Temeche, Solid Electrolytes Derived From Precursors and Liquid-Feed Flame Spray Pyrolysis Nano-Powders Enabling Assembly of All-Solid-State-Batteries, *Materials Science and Engineerin*g, University of Michigan, Michigan, USA, 2021.
[30] W. Langlar, A. Aeimbhu, P. Limsuwan, C. Ruttanapun, Microwave-assisted biosynthesis of C12A7 nanopowders from Aloe Vera leaf extract, *J. Ceram. Soc. Jpn*., 128 (2020) 322-328.

[31] D. Zagorac, J. Zagorac, M. Pejić, B. Matović, J.C. Schön, Band Gap Engineering of Newly Discovered ZnO/ZnS Polytypic Nanomaterials, *Nanomaterials*, 12 (2022) 1595.
[32] D. Jovanovic, D. Zagorac, B. Matovic, A. Zarubica, J. Zagorac, Anion substitution and influence of sulfur on the crystal structures, phase transitions, and electronic properties of mixed TiO2/TiS2 compounds, *Acta Crystallographica Section B: Structural Science, Crystal Engineering and Materials*, 77 (2021) 833-847.
[33] J. Zagorac, D. Zagorac, B. Babić, T. Prikhna, B. Matović, Effect of aluminum addition on the structure and electronic properties of boron nitride, *Journal of Solid State Chemistry*, 311 (2022) 123153.
[34] D. Fischer, D. Zagorac, J.C. Schön, The presence of superoxide ions and related dioxygen species in zinc oxide—A structural characterization by in situ Raman spectroscopy, J. Raman Spectrosc., accepted for publication, (2022).
[35] D. Zagorac, J. Zagorac, M. Fonović, T. Prikhna, B. Matović, Novel boron-rich aluminum nitride advanced ceramic materials, International Journal of *Applied Ceramic Technology*, (2022), 1-16.
[36] D. Zagorac, J.C. Schön, Chapter 8 - Energy landscapes of pure and doped ZnO: from bulk crystals to nanostructures, in: D.J. Wales (Ed.) *Frontiers of Nanoscience*, Elsevier (2022), 151-193.
[37] D. Zagorac, J. Zagorac, K. Doll, M. Čebela, B. Matović, Extreme pressure conditions of bas based materials: Detailed study of structural changes, band gap engineering, elastic constants and mechanical properties, *Processing and Application of Ceramics* 13 (2019) 401-410.
[38] D. Jovanović, J. Zagorac, B. Matović, A. Zarubica, D. Zagorac, Structural, electronic and mechanical properties of superhard B_4C from first principles, *Journal of Innovative Materials in Extreme Conditions*, 1 (2020) 12-18.
[39] J. Zagorac, D. Zagorac, D. Jovanović, M. Pejić, T. Škundrić, B. Matović, Ab initio investigations and behaviour of the α-Ce_2ON_2 phase in the extreme pressure conditions, *Journal of Innovative Materials in Extreme Conditions*, 2 (2021) 36-43.
[40] K. Hari Kumar, S. Sridar, Calphad Modelling of Ceramic Systems, *Journal of Innovative Materials in Extreme Conditions*, 2 (2021) 25-35.
[41] J. Zagorac, D. Zagorac, D. Jovanović, M. Pejić, T. Škundrić, B. Matović, Ab Initio Investigations and Behaviour of the α-Ce2ON2 Phase in the Extreme Pressure Conditions, *Journal of Innovative Materials in Extreme Conditions* 2, (2021) 36-43.
[42] D. Zagorac, K. Doll, J.C. Schön, M. Jansen, Ab initio structure prediction for lead sulfide at standard and elevated pressures, *Physical Review B*, 84 (2011) 045206.
[43] J.C. Schön, Energy Landscape Concepts for Chemical Systems under Extreme Conditions, *Journal of Innovative Materials in Extreme Conditions* 2(2021) 5-57.
[44] D. Zagorac, J. Zagorac, Advanced Semiconductors under Extreme Pressure Conditions, in: S.J. Ikhmayies (Ed.) *Advanced Semiconductors*, Springer2022.
[45] J.P. Perdew, K. Burke, M. Ernzerhof, Generalized Gradient Approximation Made Simple, *Physical Review Letters*, 77 (1996) 3865-3868.
[46] G. Kresse, J. Hafner, Ab initio molecular dynamics for liquid metals, *Physical Review B*, 47 (1993) 558-561.
[47] G. Kresse, J. Furthmüller, Efficient iterative schemes for ab initio total-energy calculations using a plane-wave basis set, *Physical Review B*, 54 (1996) 11169-11186.
[48] P. Giannozzi, S. Baroni, N. Bonini, M. Calandra, R. Car, C. Cavazzoni, D. Ceresoli, G.L. Chiarotti, M. Cococcioni, I. Dabo, A. Dal Corso, S. de Gironcoli, S. Fabris, G. Fratesi, R. Gebauer, U. Gerstmann, C. Gougoussis, A. Kokalj, M. Lazzeri, L. Martin-Samos, N. Marzari, F. Mauri, R. Mazzarello, S. Paolini, A. Pasquarello, L. Paulatto, C. Sbraccia, S. Scandolo, G. Sclauzero, A.P. Seitsonen, A. Smogunov, P. Umari, R.M. Wentzcovitch, QUANTUM ESPRESSO: a modular and open-source software project for quantum simulations of materials, *Journal of Physics: Condensed Matter*, 21 (2009) 395502.
[49] P. Giannozzi, O. Andreussi, T. Brumme, O. Bunau, M. Buongiorno Nardelli, M. Calandra, R. Car, C. Cavazzoni, D. Ceresoli, M. Cococcioni, N. Colonna, I. Carnimeo, A. Dal Corso, S. de Gironcoli, P. Delugas, R.A. DiStasio, A. Ferretti, A. Floris, G. Fratesi, G. Fugallo, R. Gebauer, U. Gerstmann, F. Giustino, T. Gorni, J. Jia, M. Kawamura, H.Y. Ko, A. Kokalj, E. Küçükbenli, M. Lazzeri, M. Marsili, N. Marzari, F. Mauri, N.L. Nguyen, H.V. Nguyen, A. Otero-de-la-Roza, L. Paulatto, S. Poncé, D. Rocca, R. Sabatini, B. Santra, M. Schlipf, A.P. Seitsonen, A. Smogunov, I.

Timrov, T. Thonhauser, P. Umari, N. Vast, X. Wu, S. Baroni, Advanced capabilities for materials modelling with Quantum ESPRESSO, *Journal of Physics: Condensed Matter*, 29 (2017) 465901.
[50] K. Momma, F. Izumi, VESTA 3 for three-dimensional visualization of crystal, volumetric and morphology data, *Journal of Applied Crystallography*, 44 (2011) 1272-1276.
[51] P. V. Sushko, A.L. Shluger, Y. Toda, M. Hirano, H. Hosono, Models of stoichiometric and oxygen-deficient surfaces of subnanoporous $12CaOx7Al_2O_3$, *Proceedings of the Royal Society A: Mathematical, Physical and Engineering Sciences*, 467 (2011) 2066-2083.
[52] N. Kuganathan, H. Hosono, A.L. Shluger, P.V. Sushko, Enhanced N2 Dissociation on Ru-Loaded Inorganic Electride, *Journal of the American Chemical Society*, 136 (2014) 2216-2219.
[53] A. Schmidt, M. Lerch, J.-P. Eufinger, J. Janek, I. Tranca, M.M. Islam, T. Bredow, R. Dolle, H.-D. Wiemhöfer, H. Boysen, M. Hölzel, Chlorine ion mobility in Cl-mayenite (Ca12Al14O32Cl2): An investigation combining high-temperature neutron powder diffraction, impedance spectroscopy and quantum-chemical calculations, *Solid State Ionics*, 254 (2014) 48-58.
[54] X. Zhang, Y. Wang, H. Wang, Q. Cui, C. Wang, Y. Ma, G. Zou, Pressure-induced amorphization in mayenite (12CaO·7Al2O3), *The Journal of Chemical Physics*, 135 (2011) 094506.
[55] L. Palacios, A. Cabeza, S. Bruque, S. García-Granda, M.A.G. Aranda, Structure and Electrons in Mayenite Electrides, *Inorganic Chemistry*, 47 (2008) 2661-2667.
[56] H. Boysen, M. Lerch, A. Stys, A. Senyshyn, Structure and oxygen mobility in mayenite (Ca12Al14O33): a high-temperature neutron powder diffraction study, *Acta Crystallographica Section B*, 63 (2007) 675-682.
[57] N. Takatoshi, H. Katsuro, K. Yoshiki, K. Toshio, H. Masahiro, T. Masaki, H. Hideo, Anion Incorporation-induced Cage Deformation in 12CaO·7Al2O3 Crystal, *Chemistry Letters*, 36 (2007) 902-903.
[58] R.D. Shannon, Revised effective ionic radii and systematic studies of interatomic distances in halides and chalcogenides, *Acta Crystallographica Section A*, 32 (1976) 751-767.